AXISYMMETRIC INSTABILITY IN A NONCIRCULAR TOKAMAK

BY

BRUCE LIPSCHULTZ

A thesis submitted in partial fulfillment of the requirements for the degree of

DOCTOR OF PHILOSOPHY

(Physics)

at the

UNIVERSITY OF WISCONSIN - MADISON

1979

ACKNOWLEDGEMENTS

I thank Stewart Prager, and am indebted to him, for the many invaluable discussions we have shared.

For his interest in my research and discussions of this thesis, I thank Clint Sprott. Others that provided helpful discussions were Dr.'s Kerst and Post. I also would like to thank Thomas Osborne for his help with early experiments and the flux plot program.

The work of Thomas Lovell, Bob Vallem, and their technical crew with the experimental equipment has been invaluable.

Last, and most importantly, I thank my wife Shelley for her patience and understanding during my graduate career, and assistance with this thesis.

TABLE OF CONTENTS

AXISYMMETRIC INSTABILITY IN A NONCIRCULAR TOKAMAK

Bruce Lipschultz

Under the supervision of

Professor J.C. Sprott and Assistant Professor S.C. Prager

The stability of dee, inverse-dee and square crossection plasmas to axisymmetric modes has been investigated experimentally in Tokapole II, a tokamak with a four-null poloidal divertor. Experimental results are closely compared with predictions of two numerical stability codes--the PEST code (ideal MHD, linear stability) adapted to tokapole geometry and a code which follows the nonlinear evolution of shapes similar to tokapole equilibria. Experimentally, the square is vertically stable and both dee's unstable to a vertical nonrigid axisymmetric shift. The central magnetic axis displacement grows exponentially with a growth time~10^3 poloidal Alfven times~ plasma L/R time. Proper initial positioning of the plasma on the midplane allows passive feedback to nonlinearly restore vertical motion to a small stable oscillation about the center. Experimental poloidal flux plots are produced directly from internal magnetic probe measurements. The PEST code, ignoring

passive feedback, predicts all equilibria to be vertically unstable with the square having the slowest growth. With passive feedback, all are stable. Thus experiment and code agree that the square is the most stable shape, but experiment indicates that passive feedback is partially defeated by finite plasma resistivity. In both code and experiment square-like equilibria exhibit a relatively harmless horizontal instability.

J. C. Sprott

S. C. Prager

CHAPTER I

INTRODUCTION

A. GENERAL OVERVIEW

The deleterious effect of impurities in tokamak plasmas has stimulated investigation of poloidal divertor configurations. The necessarily noncircular shape of these equilibria is also advantageous with respect to q[1] and β-limited MHD instabilities[2,3]. Unfortunately any deviation of an equilibrium from a circular shape may permit the plasma to be unstable to axisymmetric displacements, with toroidal mode number $n=0$. The poloidally asymmetric placement of shaping rings and walls necessary to establish a noncircular plasma shape in turn creates nonuniform attractions to the plasma current. The plasma, if perturbed, moves in the direction of the minimum in the accompanying poloidal field. Unlike kink and localized interchange modes, the axisymmetric instability cannot be controlled by increasing the toroidal field or reducing the plasma current.

Unfortunately, the conceptual simplicity of the axisymmetric instability does not translate into calculational simplicity. The importance of this mode has given rise to a fairly large amount of linear theory - mostly for idealized displacements and analytic equilibria [4-12]. Recently nonlinear evolution of the instability has been followed numerically [13]. Axisymmetric displacement of dee and elliptical plasmas has been deduced in a few experiments from magnetic probes external to the plasma[14-17]. The plasma shape in these experiments has been inferred from comparison of these same external magnetic signals with output from equilibrium computer codes. The numerical modeling of the axisymmetric instability, cited above, has apparently not been specifically applied to any of these experiments; an unfortunate gap exists between a fairly well developed theory and experiments performed.

The intent of this thesis is twofold. First, to report direct experimental observation of the axisymmetric instability in dee, inverse-dee and square shaped cross sections. Second, to compare these experimental observations with a stability code written for the actual experimental geometry. This experiment has been performed in the Wisconsin Tokapole II[18,19], a

Tokamak with a four-null poloidal divertor. Experimental magnetic flux plots for the aforementioned range of equilibria are produced, from magnetic probe measurements in the plasma interior, in detail equivalent to that provided by computer calculations. Conclusions, as to growth rates and passive stabilization, can be drawn from the time evolution of these experimental flux plots and compared with two numerical codes which closely reflect the experimental machine. The PEST code[20], which has been adapted to the Tokapole machine geometry, predicts the linear stability . The effects due to external conductors are included by appropriate vacuum modifications[21,22]. A nonlinear time dependent code, PATENT[13,23], although applied to the PDX[24] machine only, provides qualitative stability predictions and modeling of the plasma shape as a function of time. Because of the wide seperation of time scales in this experiment (e.g. Alfven, plasma and ring L/R times) many qualitative conclusions about passive stabilization can be drawn which are relatively machine independent. Qualitative comparison can also be made between experimental results and related models in the literature[19].

Several parameter variations are possible both

experimentally and numerically. For example, proper positioning of the four field shaping rings allows equilibria to be varied from dee through square to inverse-dee shaped. The dee and inverse-dee are vertically unstable when not precisely centered on the machine midplane. When vertical stability is achieved, these shapes are still horizontally unstable. The square is vertically stable even if not precisely positioned. However, this shape is also horizontally unstable. Since the horizontal instability saturates it is less harmful than the vertical displacements exhibited in the dee and inverse-dee. The vertical movement continues unrestrained towards the x-point (poloidal field null on the separatrix). Predictions of the PEST code for relative stability of these equilibria agree with experiment. Experimentally, the magnetic axis can be positioned above, below or exactly on the midplane. In both the PATENT code and experiment the plasma is seen to correspondingly move up, down or oscillate about the midplane. Both experimentally and from the nonlinear code we find the growth of the instability to be exponential in time. Ideal MHD predicts the growth time, in the absence of external conductors, to be $\sim T_a$, the poloidal Alfvén time. Experimentally, vertical and horizontal growth times are $\sim 10^3 T_a$. Passive feedback

apparently increases T_g, the growth time, from T_a to roughly the plasma L/R time. The effect of passive feedback from rings and walls is studied experimentally by changing the plasma resistivty and by varying the initial position of the magnetic axis. The instability growth time varies inversely with plasma resistivity. Stability can be numerically studied with or without rings or walls to evaluate their effect on passive stabilization.

In section B of this chapter an attempt is made to give the reader an intuitive feel for the physical nature of axisymmetric instabilities. Chapter II includes a description of the experimental machine (II.A) and techniques (II.B), as well as a review of previous (II.C) and present (II.D-F) experimental results. Chapter III is devoted to theory. After a review of previous theoretical work (III.A), the numerical codes used in this study are described (III.B-D) and their predictions reviewed (III.E-F). Experimental and theoretical results are discussed and compared in Chapter IV with a summary in table 1.

B. Physical Intuition

The physical nature of the axisymmetric instability can be illuminated through intuitive means. At first we will assume that currents in the plasma and external conductors are fixed. Also, for simplicity, we will discuss linear as opposed to toroidal geometry. Allowance for toroidal curvature introduces a force produced by the inductive interaction of the plasma current with its self magnetic field. This force tends to increase the plasma major radius and is different in nature from the axisymmetric instabilities discussed here.

It is illustrative to study a stable equilibrium and then relate what actions must be taken to create an unstable one. This simple situation of a linear tokamak plasma is illustrated in figure 1a. We see, for this circular shape with return current at infinity, there is no preferred direction, i.e. there are no currents or magnetic fields for the plasma current to interact with. Thus it is neutrally stable with respect to a rigid displacement; given a perturbation it will keep travelling at a constant velocity. This neutral stability to displacements can be modified to instability

Figure 1: Illustration of the relation between deformation and stability in a linear geometry. All three plasma crossections include 'toroidal' current into the paper. a) Neutrally stable circular plasma extending into paper. b) Elliptical plasma deformed from circle by currents I_1 & I_2. The attractive forces, F_1 & F_2, between the plasma current and each shaping rod are balanced. c) Same elliptical plasma displaced vertically. F_1 & F_2 are no longer balanced - vertical displacement grows.

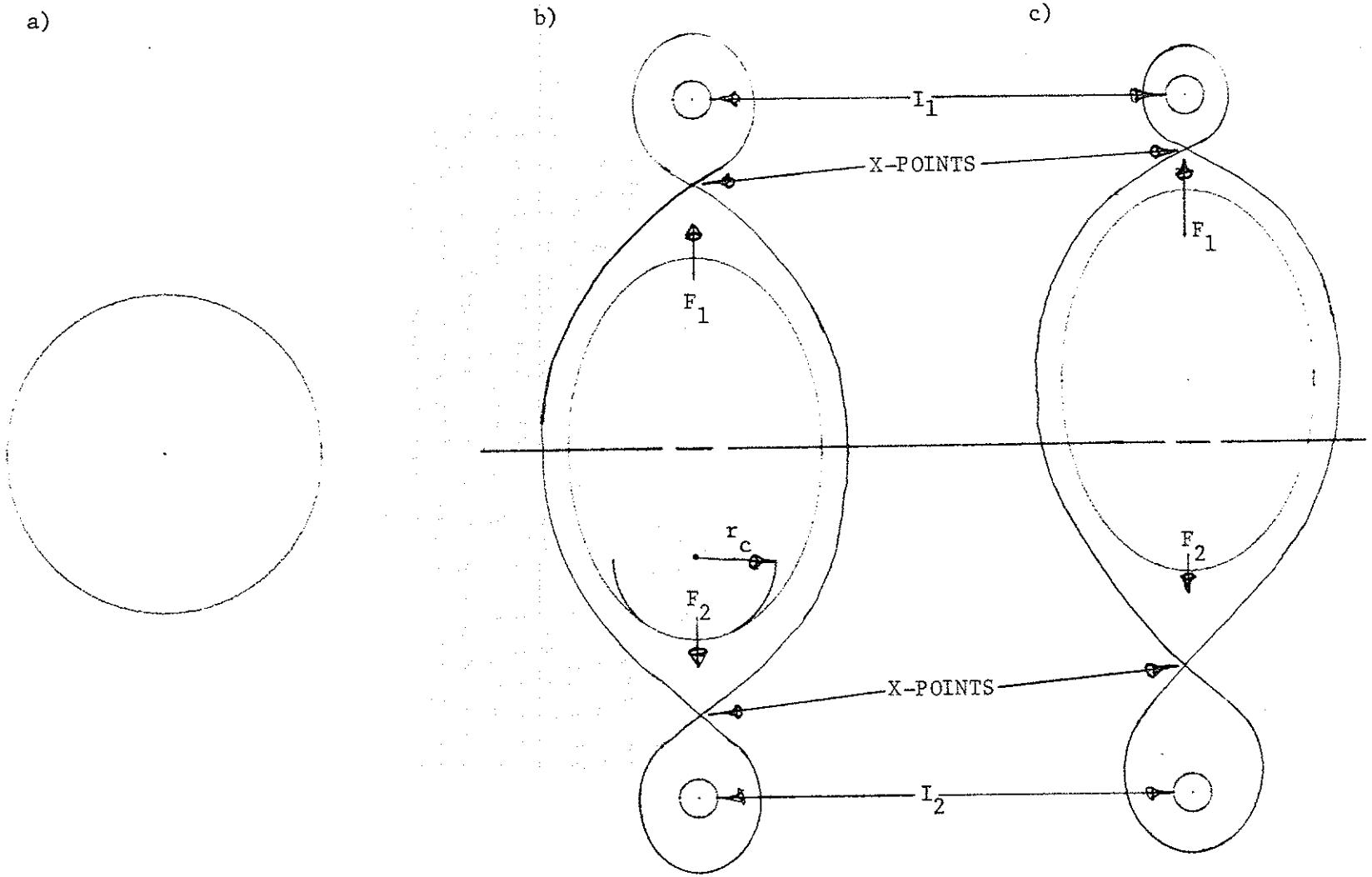
a)
b)
c)
I_1
X-POINTS
F_1
F_1
r_c
F_2
F_2
X-POINTS
I_2

by deforming the plasma to a noncircular shape using external currents (fig. 1b). Here the plasma current can interact with the shaping currents, absent in the circular case. This attraction is the characteristic driving force of what is generally called the vertical 'axisymmetric' instability. The word 'axisymmetric' in this linear situation connotes an axially symmetric movement of the entire plasma column, with axis into the paper. When this ellipse is positioned precisely between the two shaping currents, the forces F_1 and F_2, between the plasma and shaping currents, are balanced. If the ellipse is perturbed vertically away from this point, F_1 and F_2 become unbalanced, and instability growth ensues (fig. 1c). No great leap of the imagination is needed to see that increasing the deformation (ellipticity) will increase the instability growth rate. The attraction is greater because: 1. The shaping currents are larger and, 2. The plasma is in closer proximity to these currents. The increase in deformation can best be characterized by a decrease in the poloidal field radius of curvature; r_c, near the x-point (see fig. 1b).

This same prescription: decreasing r_c ~ increasing deformation ~ plasma more unstable to displacements, can be applied to other shapes. In the presence of an

octupole field (fig. 2a), a square cross section plasma will be more stable to displacements in the direction of an octupole current than either a dee or inverse-dee. The latter two shapes are equivalent in a linear geometry. In comparison to the square, the dee of equivalent current is closer to either pair of z-symmetric shaping current conductors. Also these closer currents must be increased to initially create the dee. Thus the dee will experience greater attractive forces. The more unstable shape again has the greater deformation or smaller r_c. The dee, when perturbed upward (downward) will move towards the upper (lower) closest octupole current. The attractive force increases as the dee moves closer. Figure 2b illustrates the situation. Although this is what is generally denoted a vertical instability a more apt name that I will use in this discussion is x-point instability. The attractive force that drives this instability is always between two like currents that generate a field null (x-point).

The role of the plasma current distribution is important to these instabilities. A flat current distribution is more unstable than a parabolic profile for approximately the same plasma shape and total current. There is more plasma current in closer

a)

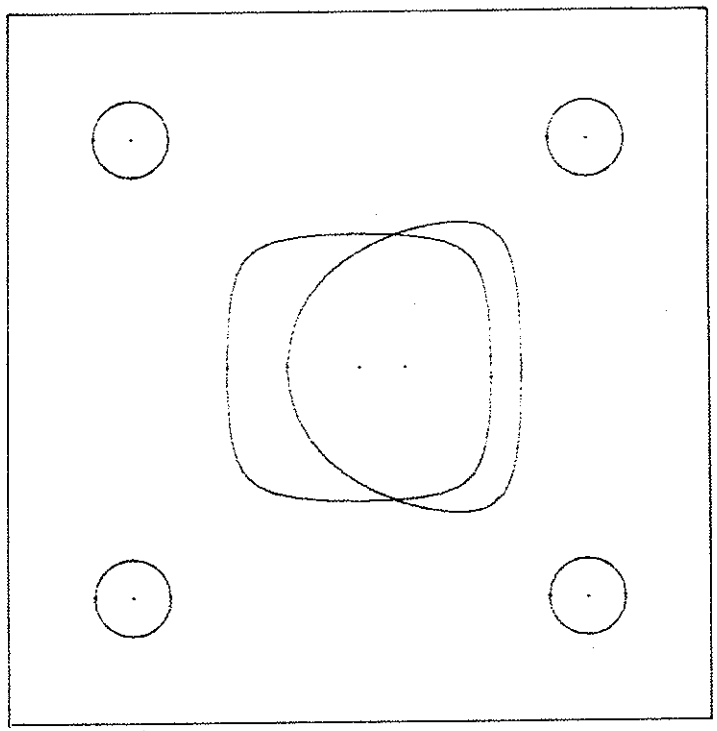

b)

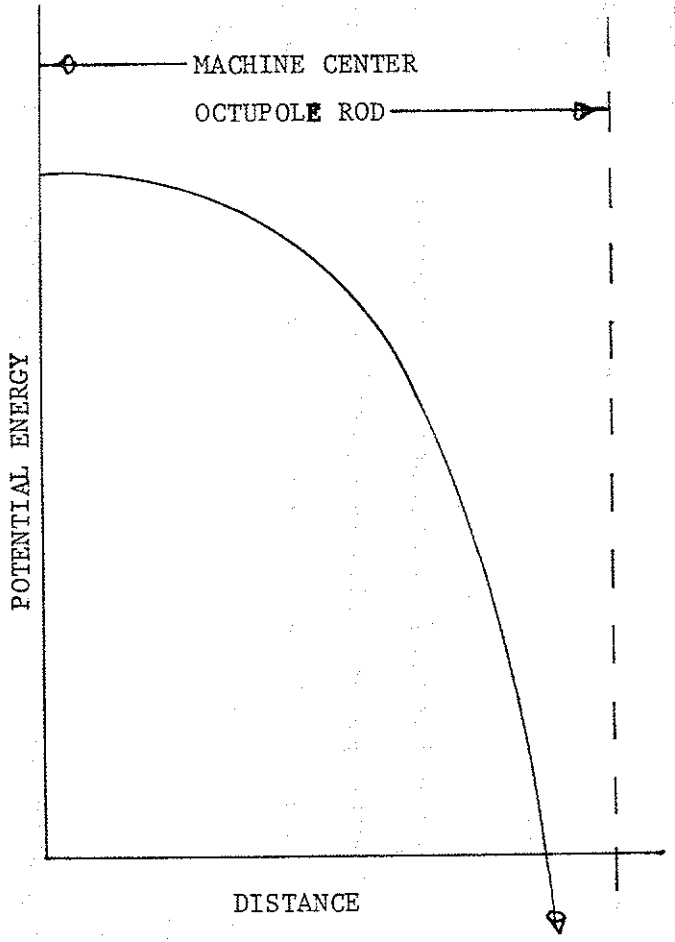

Figure 2: A further illustration of the x-point instability in a linear geometry. a) The inverse-dee is closer to shaping rods than square. b) Potential energy vs. distance to the attracting rod.

proximity to the shaping currents. The attractive force is $\propto 1/r$, where r is the relative distance between the currents involved.

Understanding horizontal (equivalent to vertical direction in a linear device) displacements is not as straightforward as the x-point instablity. If a toroidal current filament were placed centrally in a linear octupole field, it would be horizontally stable. Designating the toroidal direction as into the paper, then examination of the $\underline{I}_{fil}\underline{x}\underline{B}_{pol}$ force at points along the midplane, for this test current and vacuum poloidal magnetic field, reveal a restoring force that increases monotonically with minor radius. A potential energy curve, illustrating this effect, is drawn as a function of distance along the midplane in figure 3a. Note this curve is shallower than that for the x-point direction (fig. 2b) because the octupole rods are closer to machine center than the image currents that represent the wall. A plasma is not a current filament: we must take into account the sum of forces over the plasma cross section. Furthermore, the plasma is a cohesive entity described by the MHD equations. Figure 3b exhibits this force field, experienced by a filament test current, for one quadrant of the octupole field. The

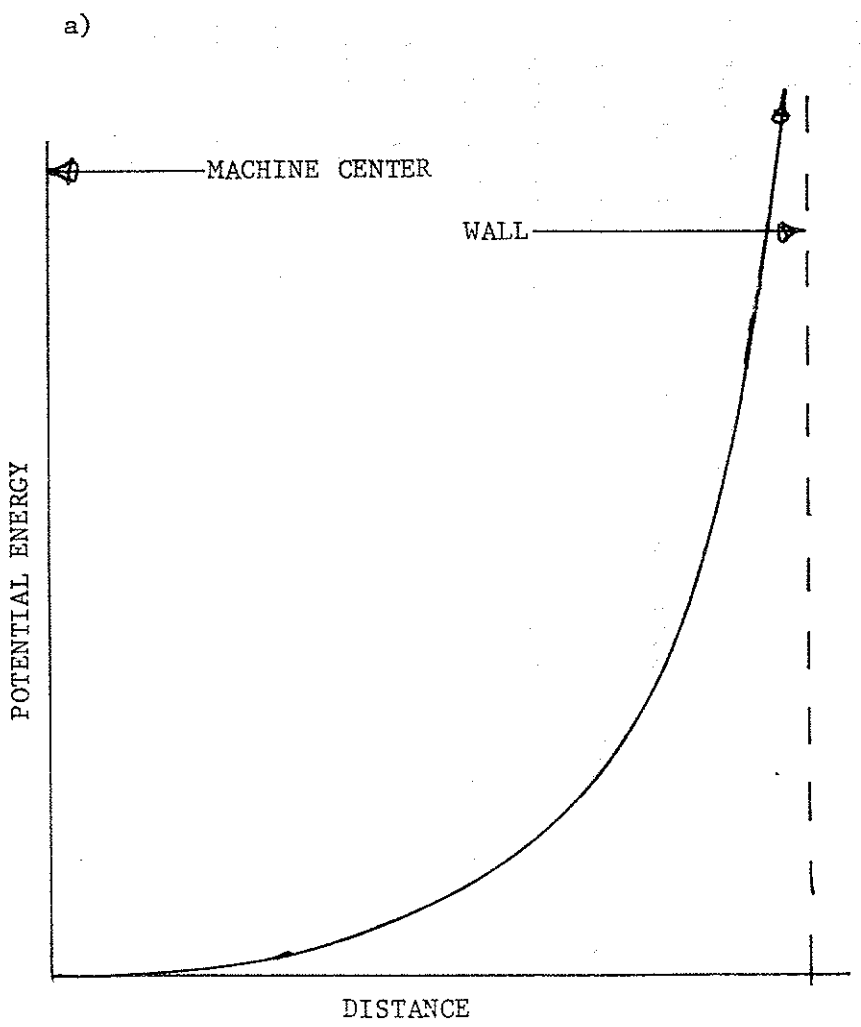

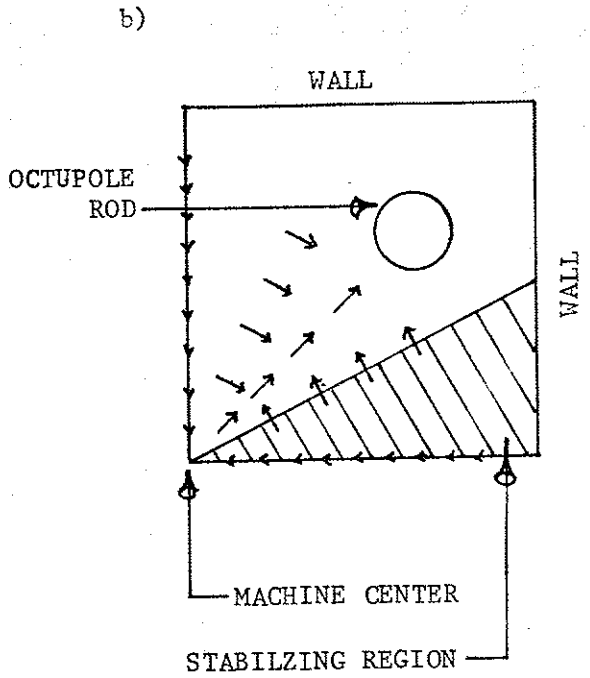

Figure 3: Illustration of the horizontal instability in an octupole geometry. a) Potential energy vs. distance to the wall. b) Force field of a filament test current in one quadrant of octupole. Shaded area has a horizontally stabilizing influence.

complete flux plot from which this figure is derived is shown in fig. 5. Since, in linear geometry, all quadrants are equivalent only one is shown in fig. 3b. The area that repels horizontal movement is shaded. Comparing the square shape, placed at machine center, to the inverse-dee, displaced to the right, the square contains less of the horizontally stabilizing region than the inverse-dee. Therefore, the square is least stable to horizontal as opposed to x-point displacements.

Up until now, we have treated the plasma and external conductors as having fixed currents during displacements. If the currents involved are allowed to react to the plasma motion, passive stabilization can occur. Let us first treat the idealized case of two parallel currents with the constraint that their total flux be held constant during movement (fig. 4). Ignoring reconnection (i.e. for an infinitely conducting plasma at the x-point), if they are allowed to move towards each other, field lines will be compressed and the integral of $\underline{B}\cdot\underline{dl}$ around each rod will increase. Antiparallel currents will be correspondingly induced to keep this integral a constant. Thus the currents are reduced causing the attractive force, $2I_1I_2/r_{12}c^2$, and growth rate to decrease. This effect, of induced

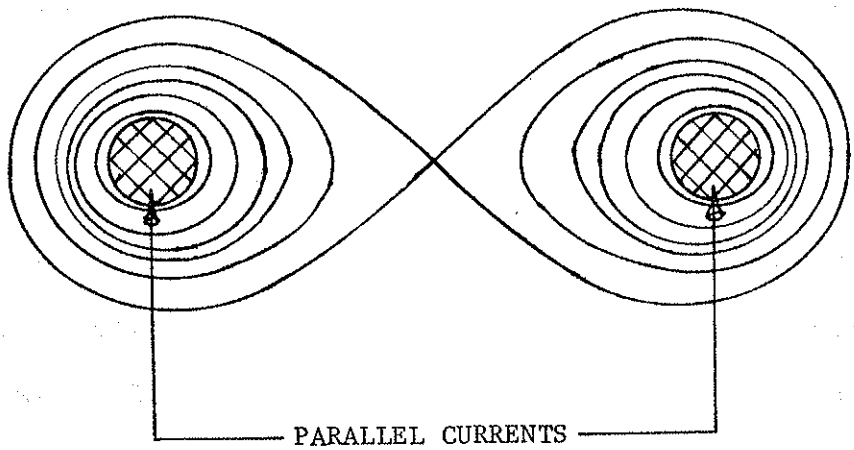

Figure 4: Two parallel linear (into paper) currents with accompanying quadrupole magnetic field.

currents slowing the movement, is termed passive stabilization.

There are two complicating factors that can affect the efficiency of passive stabilization. The first to be discussed is finite resistivity in the conductors. Compressed flux can be pushed through the rods on a soak-in time scale T_{soak} proportional to the square root of conductivity. The net effect is that induced stabilizing currents will decay over time. Thus, if a movement (instability) could be stabilized by rods of infinite conductivity, then allowing finite resistivity enables the instability to grow with a rate~$1/T_{soak}$.

The other factor in passive stabilization is the presence of plasma. In a vacuum field, lines can reconnect instantly. In the presence of plasma, line reconnection occurs at a rate $\propto 1/T_{res}$. T_{res} is the characteristic resistive decay time of the plasma. Thus, additional flux compression can occur, slowing the instability growth rate.

If we apply the concept of passive stabilization to the case of the x-point unstable dee in an octupole field, the plasma and nearest rod are the primary

currents involved. There is also, of course, plasma at the x-point. Some passive stabilization will occur but full stabilization is not neccesarily possible. If we bring into this discussion the effect of conducting elements other than those primarily involved, then passive stabilization will be more effective. Flux decompression, with accompanying induced attractive currents, will occur in the other conductors (e.g. the other three rods and opposite walls). The efficiency of induced effects will not only be determined by the characteristic resistive decay time scales involved, but on the amount and proximity of induced currents as well. The dee is in closer proximity to fewer rings and walls than the square of equivalent total current. Therefore, passive stabilization will be more effective for the square than for the dee. In either case, if the plasma is not completely stabilized, then the growth time will be slowed to the order of the minimum of the resistive time scales involved.

Not discussed, heretofore, is the relation of the 'toroidal' field to the axisymmetric instability. Intuitively, it must play a much smaller role than the poloidal field. The deformation will stretch the poloidal field on the order of a minor radius-scale

length. On the other hand, the toroidal field is only slightly deformed while the entire field line is being pushed out of the way, either up or down. There may be some horizontal stretching to this movement but it is on the order of the major radius. Thus, the displacement divided by the scale length involved is smaller for the toroidal field. In addition to this small contribution of the stretched toroidal field, there is the effect of its gradient introduced by toroidality. In equilibrium, by definition, the $\underline{J}_{pol}{}^{x}\underline{B}_{tor}$ force is balanced everywhere by $\underline{J}_{tor}{}^{x}\underline{B}_{pol}$ (for low pressure). When the plasma becomes unstable, this condition may perhaps no longer hold. Examination of the $\underline{J}_{pol}{}^{x}\underline{B}_{tor}$ force near the principal x-point involved, shows that the force increases as major radius R decreases. The introduction , therefore, of toroidal curvature can perhaps differentiate between the two dee's making the dee slightly more unstable than the inverse-dee.

In summary, through the application of basic physical concepts, we can see that increased deformation (decreasing r_c) indicates a shape to be relatively more unstable toward x-point displacements. This implies the square is more stable than the dee or inverse-dee. Passive feedback stabilization can either completely

stabilize this movement or at least slow its growth to the resistive time scales involved. Its effectiveness should be greater for the square than for the dee's. The relative stability of these shapes becomes reversed when discussing horizontal displacements. The effect of toroidal field, though all important for higher n (toroidal mode number) instabilities, has only a minor influence on the stability of the axisymmetric modes (n=0).

CHAPTER II

EXPERIMENT

A. Machine Description

The Tokapole II device[18], on which these experiments were performed, has a 50 cm. major radius square cross section (44 x 44 cm.) vacuum chamber. The vacuum magnetic flux plot is that of an octupole (fig. 5a), which provides vertical and horizontal fields to center the discharge. The octupole vacuum poloidal field is produced by inductively driving, through an iron core linking the toroid, four 5 cm. diameter copper toroidal rings. These rings can carry up to a total of 700 kA, and are each supported by three copper-beryllium rods. While the chamber is under vacuum the rings can be moved vertically ±5mm. by external means. When plasma current is driven toroidally through the octupole null, a tokamak with a four-null divertor is generated (fig. 5b).

Electrical characteristics are shown in figure 6. The current in an outer ring rises sinusoidally to 45 kA (fig. 6a). A 1 msec. pulse of 10 kW. 8.8 GHz

Figure 5: Numerical poloidal flux plots (major axis to left). a) Without plasma. b) With plasma. Each tic mark indicates 2 cm.

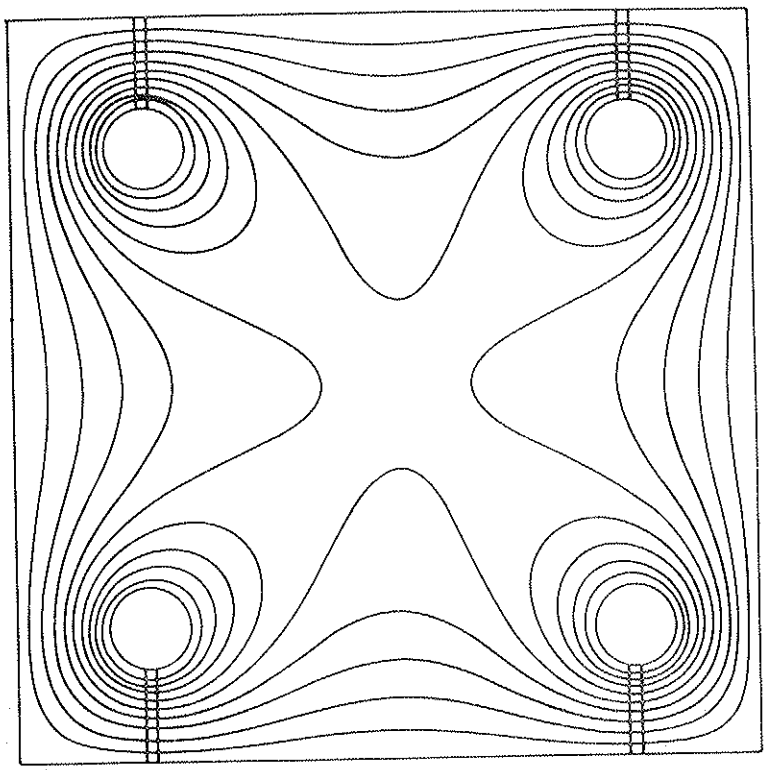

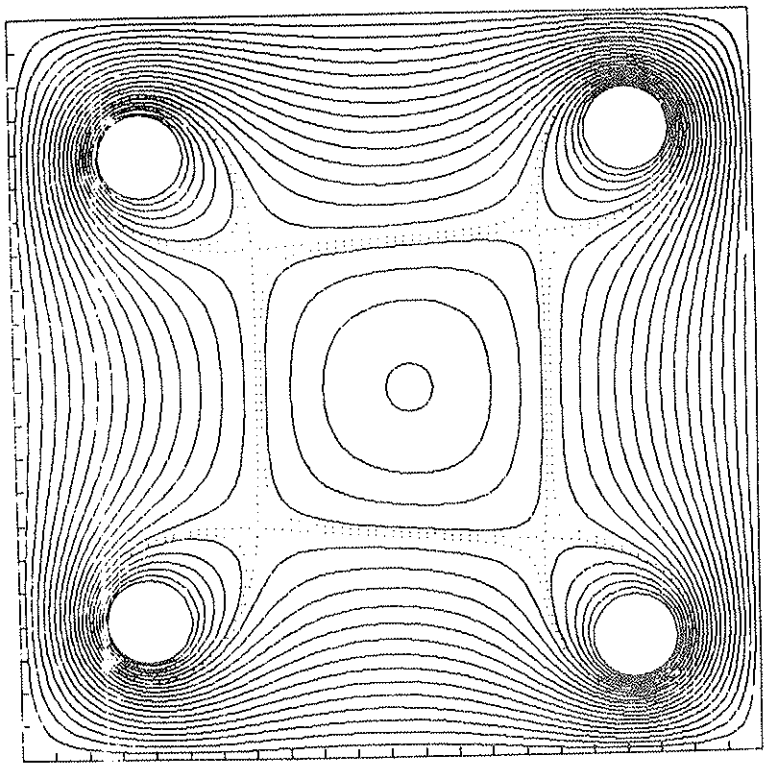

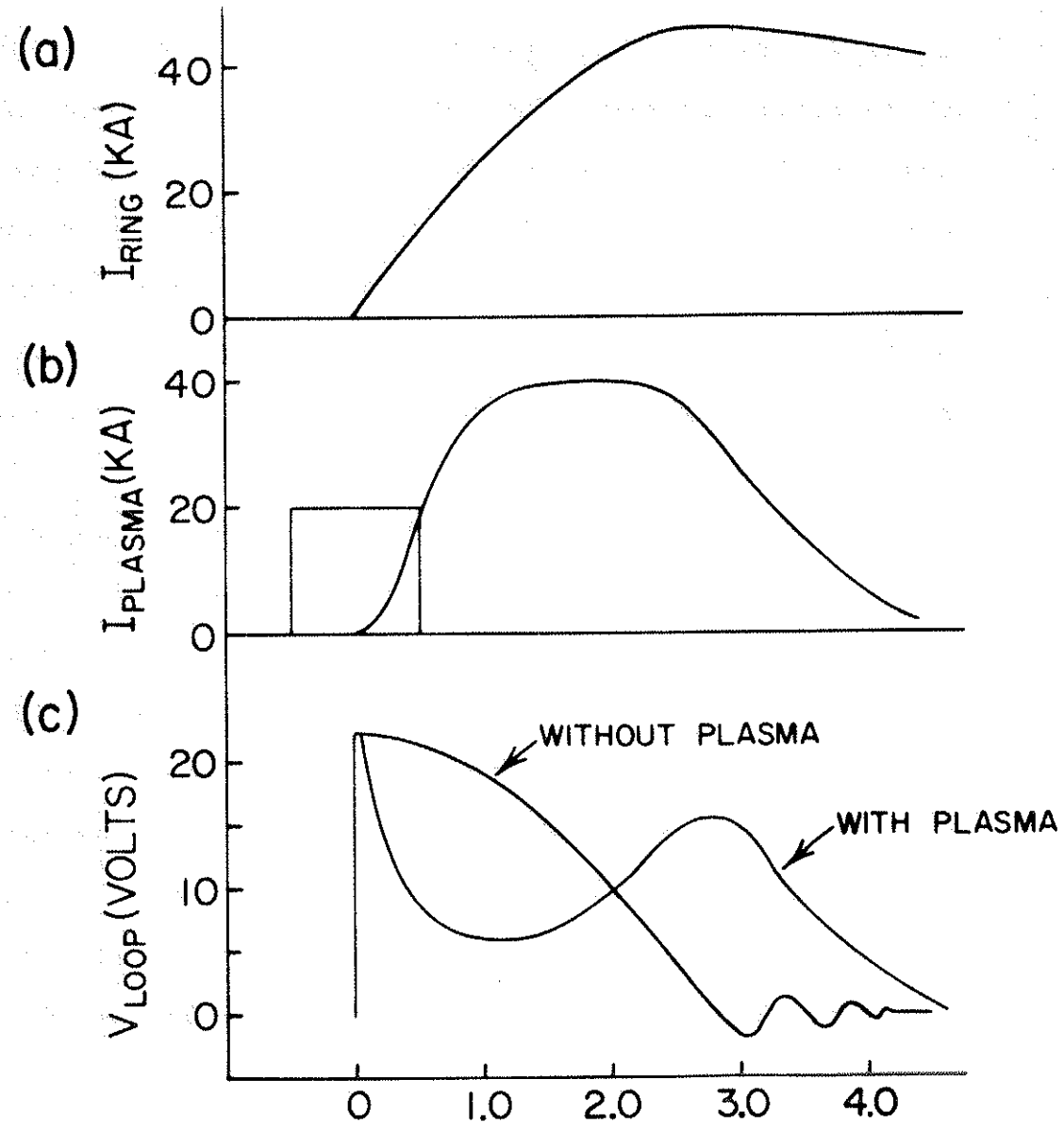

Figure 6: Electrical characteristics. Time, in ms., is given on abscissa. a) Current in an outer ring vs. time. Also shown is a 10 kW, 8.8 GHz, 1 ms. microwave preionization pulse. b) Plasma current. c) Loop voltage at machine center with and without plasma.

microwaves is used for preionization (fig. 6b). The plasma current is induced by the same source as the ring current. The value for the total toroidal plasma curent is inferred from measurements of the poloidal field transformer primary current and loop voltage, at the wall, employing a simple model treating the plasma and rings as coupled inductors[25,26]. The current inside the separatrix is also calculated from measured magnetic flux plots. The peak total plasma current is ~ 40 kA with ~ 4 msec pulse length (fig. 6b). The toroidal field is effectively constant during the experiment at a value of 3.2 kG at machine center, with capability of up to 8.5 kG. The vacuum toroidal loop voltage (fig. 6c) at machine center decays as a cosine to zero in ~ 3 msec and is then crowbarred. In the presence of plasma the loop voltage is depressed during plasma current rise and enhanced during current decline due to the back EMF self-induced by the plasma current. Peak electron temperatures are ~ 100 eV surmised, with ~ 25% accuracy, from modeling of the time evolution of a set of impurity lines (e.g. OI-OVI). The electron density is ~ 10^{13} cm^{-3} as measured by microwave interferometry and Langmuir probes. The ion temperature varies from 20-70 eV as determined by charge-exchange analysis and from the doppler broadening of He II.

B. Experimental Techniques

The basic information without which this research would not be possible is the poloidal magnetic flux plot. The tool used for obtaining a flux plot is the '$\dot{B}$' probe - so termed because the output is proportional to the time derivative of magnetic flux at the probe tip. The '$\dot{B}$' probes used in these experiments consist of two 40 turn, 4x4x5 mm coils of wire, located at the sealed end of a 1/4 inch tube. The coils are wound on top of each other and have normals parallel and perpendicular to the probe length. The orientation allows both components of poloidal magnetic field to be resolved. The frquency response of this probe varies between 100 kHz. and 1 mHz. depending on the exact number of turns and areas of the coils.

After passive integration, each probe signal is digitized and stored by computer. To correct for probe misalignments at a given point, a discharge with only the toroidal field is stored and subtracted from the data with both magnetic fields and plasma. After this

correction, the probe signal every 50μs, for 4 msec., is stored on floppy disk for further analysis.

The expression used to calculate the poloidal flux, ψ is

$$\psi = \int_0^r dr' \; 2\pi(R_0+r')B_{perp}(r') \qquad (2.1)$$

where R_0, r' and B_{perp} are the major radius of the magnetic axis, the minor radius and the poloidal field component perpendicular to the path of integration respectively. Surfaces of constant ψ are generated from the magnetic field data measured at 90 spatial points on a 2 cm by 2 cm grid (fig. 7a). Within any six point rectangular grid area, or r.g.a. (same figure), the vertical and horizontal poloidal magnetic field components are fit to a polynomial of the form

$$B(x_i,y_i) \sim A^i y_i^2 + B^i x_i y_i + C^i x_i + D^i y_i + E^i \qquad (2.2)$$

where A^i, B^i,....., E^i are the coefficients for the i^{th} r.g.a. $B(x_i,y_i)$ is either the first or second component, vertical or horizontal, of the magnetic field at the local coordinates (x_i,y_i) within the i^{th} r.g.a. From

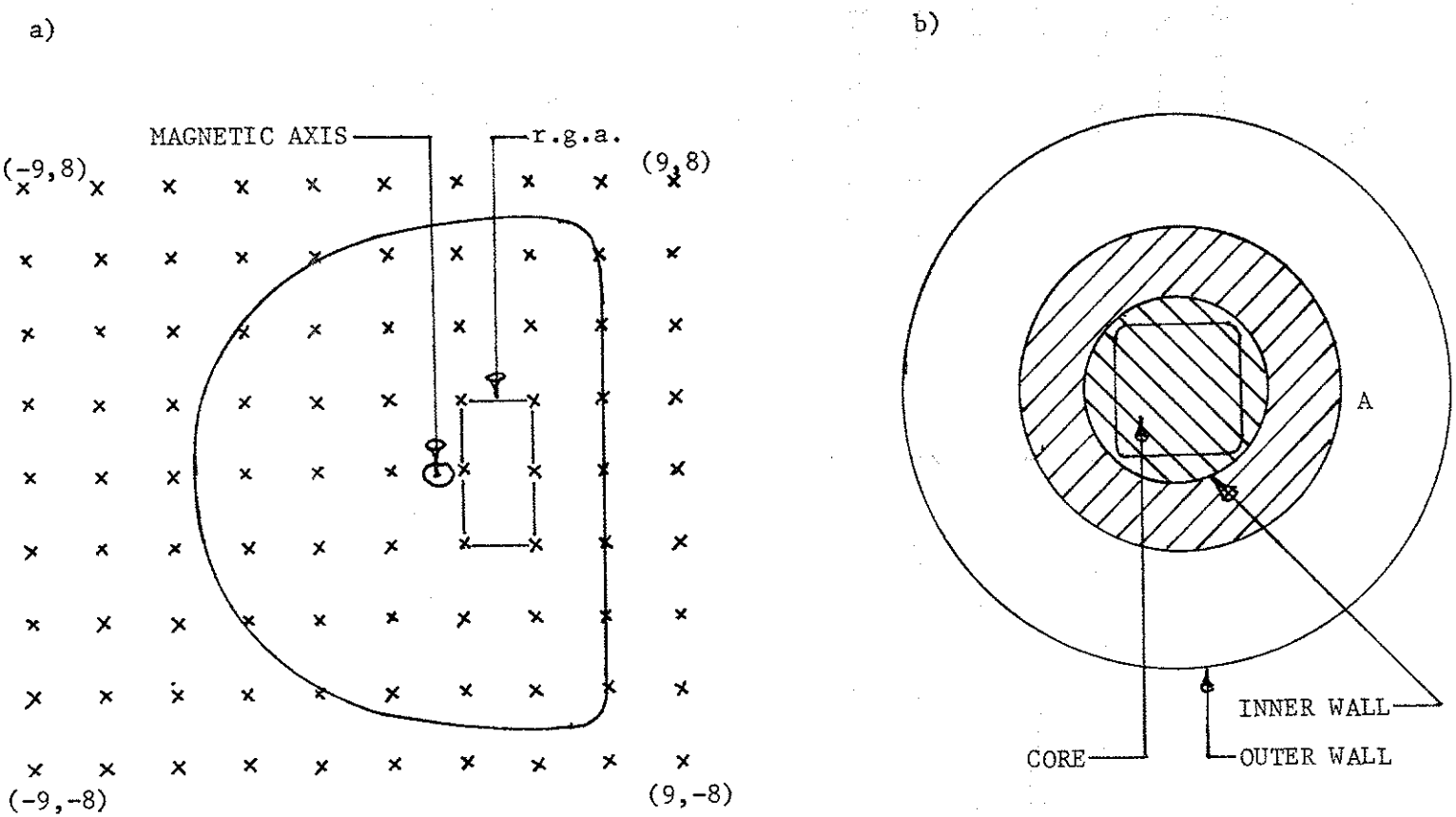

Figure 7: Experimental techniques. a) Data grid (2 cm. spacing) for magnetic flux plots.
b) Top view of experimental machine.

equations (2.1) and (2.2), an explicit polynomial in x_i and y_i can be found for ψ,

$$\psi(r,\theta) = \psi^i(x_i, y_i, x_{i0}, y_{i0}, A^i_{1,2}, B^i_{1,2}, \ldots, E^i_{1,2}) + \psi^i_0 \tag{2.3}$$

where ψ^i_0 is the value of ψ at the edge of the r.g.a. of position (x_{i0}, y_{i0}) relative to the magnetic axis ($\psi(0,\theta)=0$). The subscript 1,2 on the magnetic field coefficients refer to the vertical or horizontal components of the poloidal field. Thus, once the position of the magnetic axis is known, the approximate value of ψ along a ray out from the axis is obtained in a stepping fashion. ψ^i_0 is determined by the final value obtained in integration through the previous r.g.a. out along that ray.

The position of the magnetic axis is found numerically by first searching for the data point with minimum B^2. This point and the eight surrounding it, define two r.g.a.'s, j-1 and j. Using explicit forms for

$$\frac{\partial \psi^j}{\partial x_j}, \quad \frac{\partial \psi^j}{\partial y_j}, \quad \frac{\partial^2 \psi^j}{\partial x_j y_j}, \quad \frac{\partial^2 \psi}{\partial y_j^2}, \quad \cdots \tag{2.4}$$

the first order Taylor series expansion for ψ^j is

iterated to find $\nabla\psi=0$. Five iterations are usually sufficient for convergence.

After the magnetic axis is found, the program generates an array $\psi_{sav}(k)$ containing the value of flux every 4 mm along a horizontal ray from the axis to the edge of the data grid. Then, every 5 degrees around the axis, the program searches for the radius at which $\psi(r(k,\theta))=\psi_{sav}(k)$. These values of $r(k,\theta)$ define a flux surface.

Once the locus of points defining a flux surface is determined, various line integrals over the flux contours are approximated using Newton's 3/8 rule. The safety factor q(k), toroidal current I(k) and area A(k) within the k^{th} closed flux surface are given by

$$q(k) = \frac{1}{2\pi}\int_{\{r(k,\theta),\theta\}} \frac{rB_\phi}{RB_\theta}\, d\theta$$

$$I(k) = \frac{1}{\mu_0}\int_{\{r(k,\theta),\theta\}} B_\theta r\, d\theta$$

$$A(k) = \int_{\{r(k,\theta),\theta\}} r^2\, d\theta \qquad (2.5)$$

The last step is to compute the toroidal current

density averaged over the annulus between two flux surfaces,

$$J(k)=[I(k+1)-I(k)]/[A(k+1)-A(k)] \qquad (2.6)$$

Another diagnostic that is important to this study is the electric field probe. This consists of a few turn coil of wire 4 mm wide by 50 cm in length. As in the case of the $\dot{B}$ probe, the coil is contained in a 1/4 inch probe tube. The principle by which it works is illustrated in figure 7b. The output is proportional to the time derivative of the poloidal magnetic flux through the coil. Assuming the poloidal field to be sinusoidal in time, then the probe signal is a measure of the flux between the toroidal circle A, that its tip defines, and the machine wall. Let us designate this flux ϕ_{probe} (see fig. 7b). The toroidal electric field at A, though, is proportional to the amount of flux between it and the core = $(\phi_{probe} - \phi_{wall})$. The flux linked by the wall, ϕ_{wall}, is opposite in direction. Converting this formula to measurable voltages we see

$$V_{loop} = V_{probe} - V_{pg} \qquad (2.7)$$

where V_{pg} is the poloidal gap voltage ($\propto \phi_{wall}$), and $V_{probe} \propto \phi_{probe}$. In actual use, care must be taken to insert the probe only on the midcylinder so that there is no component of toroidal electric field along the long sections of the coil. For the same reason the other end of the coil must be outside the machine.

C. Previous Experimental Work

Experiments heretofore performed on noncircular tokamaks have included doublets[27], ellipses[14,16] and dee's[14,16,17]. Verification of the shapes studied has occurred through external means. For example, in TOSCA[14,16], external magnetic field signals were compared with a computer model's predictions for those signals. Another variation, used on doublets and TOSCA, is the use of measured winding currents combined with appropriate plasma parameters to model the plasma. The existence of certain poloidal modes of the tearing instability has also proved to be useful in determining q, which thru the assumption of ellipticity, in turn determines the plasma shape[28]

Although existence of these equilibria has been shown in only a few papers, the stability of shapes to axisymmetric modes is even less documented. Both Toyama[17] and Bhatnagar[29] have verified the instability's existence in their respective machines, but that is the extent of their study. Bhatnagar considered the instability as a problem to be controlled, not studied. He found that the discharge length could be doubled by proper active feedback stabilization. The only major experimental study of the axisymmetric instability, previous to the present, was performed in TOSCA.

The shape of TOSCA's different equilibria is found by comparing external experimental data with predictions of an ideal MHD calculation. The experimental input consists of plasma and winding currents in addition to a limiting wall. Plasma movement, both radial and vertical, is calculated using a model that assumes the plasma to be a current filament. The difference in magnetic field, due to plasma current only, on opposite sides of the plasma gives the relative position of a current filament between those two machine sides. Cima predicts that the filament model only leads to errors of $\lesssim 3$ mm in predicting the magnetic axis position! Using this technique of locating the magnetic axis as a

function of time, growth rates of the instability are generated. No comment is given to explain how, and when during instability growth, the growth rate is derived. This has the added consequence of shedding no light on the instability's non-linear or linear nature.

An effort was made to compare their results with related analytic and numerical studies in the literature, which were not performed for TOSCA. The plasma equilibrium is described quantitatively by the decay index $n=-R/B_z(dB_z/dR)$ averaged over the plasma volume. This average is performed using the vacuum poloidal field of the winding currents. The averaged decay index $\bar{n}$ is found to be a monotonic function of ellipticity (e). Results indicate that there are certain $\bar{n}$, or e, parameter limits beyond which no stable equilibria exist. When the equilibrium is unstable, they find its growth rate to be proportional to the shaping currents. In other words, increasing the amount of noncircular deformation decreases plasma stability. Indications are given that T_g is increased by the presence of the passive feedback coils.

D. Relative Stability of Dee, Inverse-dee and Square Equilibria

This experiment allows comparison of various plasma shapes in one machine under similar conditions. By varying the placement of the rings, which attract the plasma, the shape of the tokamak separatrix can be changed from dee to inverse-dee (figures 8a-c). If the inner rings are moved closer together, and thus nearer the plasma, the equilibrium is positioned slightly inward in major radius producing a dee (fig. 8a). An inverse-dee (fig. 8b) is created by positioning the outer rings closer together. The intermediate case is a square plasma (fig. 8c). Previous experiments concerning noncircular tokamaks have deduced the plasma shape using external measurements such as winding currents, plasma current and edge magnetic fields, combined with computer modeling. All important data in this paper, such as flux plots, current density and electric field profiles are deduced from internal probe measurements. A description of these experimental techniques is given in the previous section (III.C).

The time histories of magnetic flux plots show that the dee and inverse-dee are unstable to a non-rigid

Figure 8: Experimental flux plots mapped out with magnetic probes. Only the area inside the separatrix is shown. Each tic mark indicates 2 cm. a) Dee. b) Inverse-dee. c) Square.

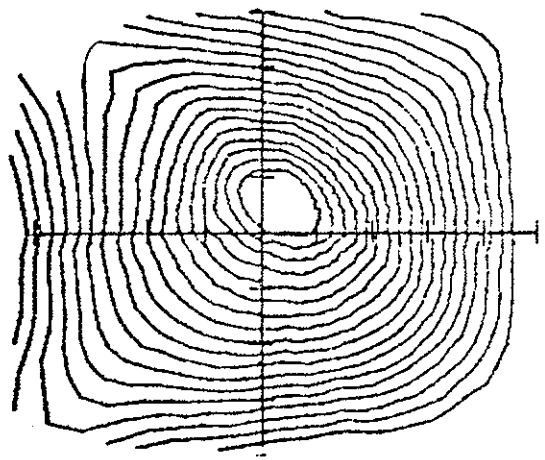

A

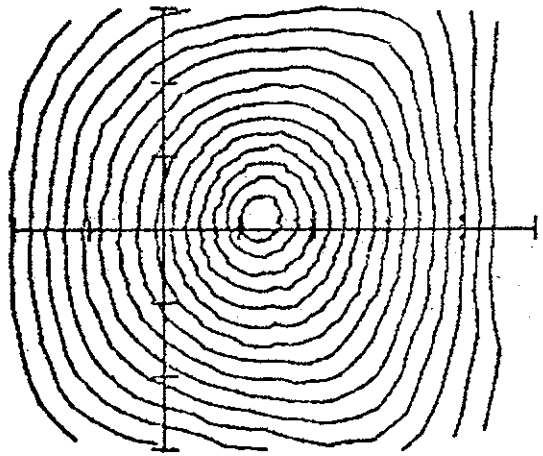

B

vertical movement, along a line of sight from the magnetic axis to a ring (figure 9). The square is stable to this movement on the time scale of this experiment. For the vertically unstable shapes, a plot of the magnetic axis position, shown in figure 10, indicates that the vertical displacement increases exponentially with a growth time $T_g \sim 450$ usec. $T_g \sim 10^3 T_a$, where T_a is a poloidal Alfvén time calculated with a suitably averaged poloidal field. It is also interesting to note, and will be discussed later, that T_g is much less than the resistive decay time of rings and walls (15 msec) and very close to the plasma L/R time ($\sim$ .5-2.0 msec). Axisymmetry has been verified at several machine azimuths. Also, the effect of plasma outside the separatrix has been examined: That plasma was wiped out by a movable limiter. The resulting instability growth rate and equilibrium shape were identical to the 'normal' case, within experimental uncertainties.

We find that all these equilibria can be stabilized to vertical movement, on the time scale of this experiment, by precise positioning of the rings. After the vertical movement is stabilized there still remains a horizontal motion that is independent of the rise and fall of the plasma current. This horizontal instability

Figure 9: Time evolution of the experimental flux plot for a) inverse-dee & b) square. The dee evolves similarly to inverse-dee.

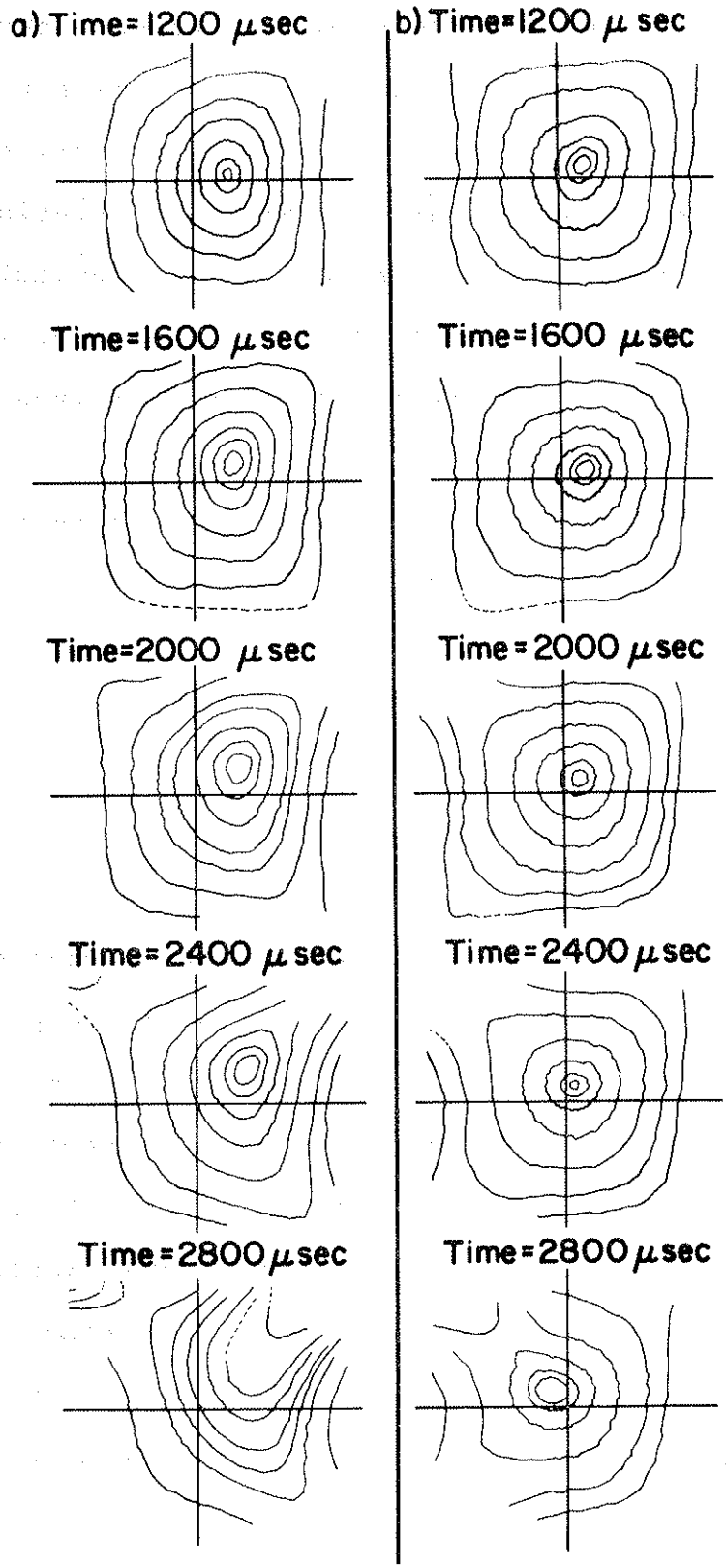
a) Time= 1200 μsec
b) Time=1200 μ sec
Time=1600 μsec
Time=1600 μsec
Time=2000 μsec
Time = 2000 μsec
Time=2400 μsec
Time=2400 μsec
Time=2800 μsec
Time=2800 μsec

occurs in the square as well as the dee and inverse-dee. The direction of this motion depends strictly on which set of rings the inner plasma separatrix encircles. When the plasma "leans" on the outer (inner) set of rings the movement is towards increasing (decreasing) major radius. Growth times for this horizontal instability, like the vertical, are $\sim 10^3 T_a$. Thus a plot of the magnetic axis position vs. time for horizontal movement is identical to that shown for the vertical (fig. 10). This horizontal instability does not saturate on the time scale of the experiment.

E. Effect of Plasma Resistivity

The role of passive stabilization could be all important to this instability and perhaps in practice eclipse distinctions based on plasma shape. Since the rings are inductively driven, there are no external circuit connections between them. Thus they are free to independently respond to the plasma motion. However, the efficacy of passive feedback, arising from induced image currents flowing in external conductors and plasma, is limited by the finite resistivity of the the elements

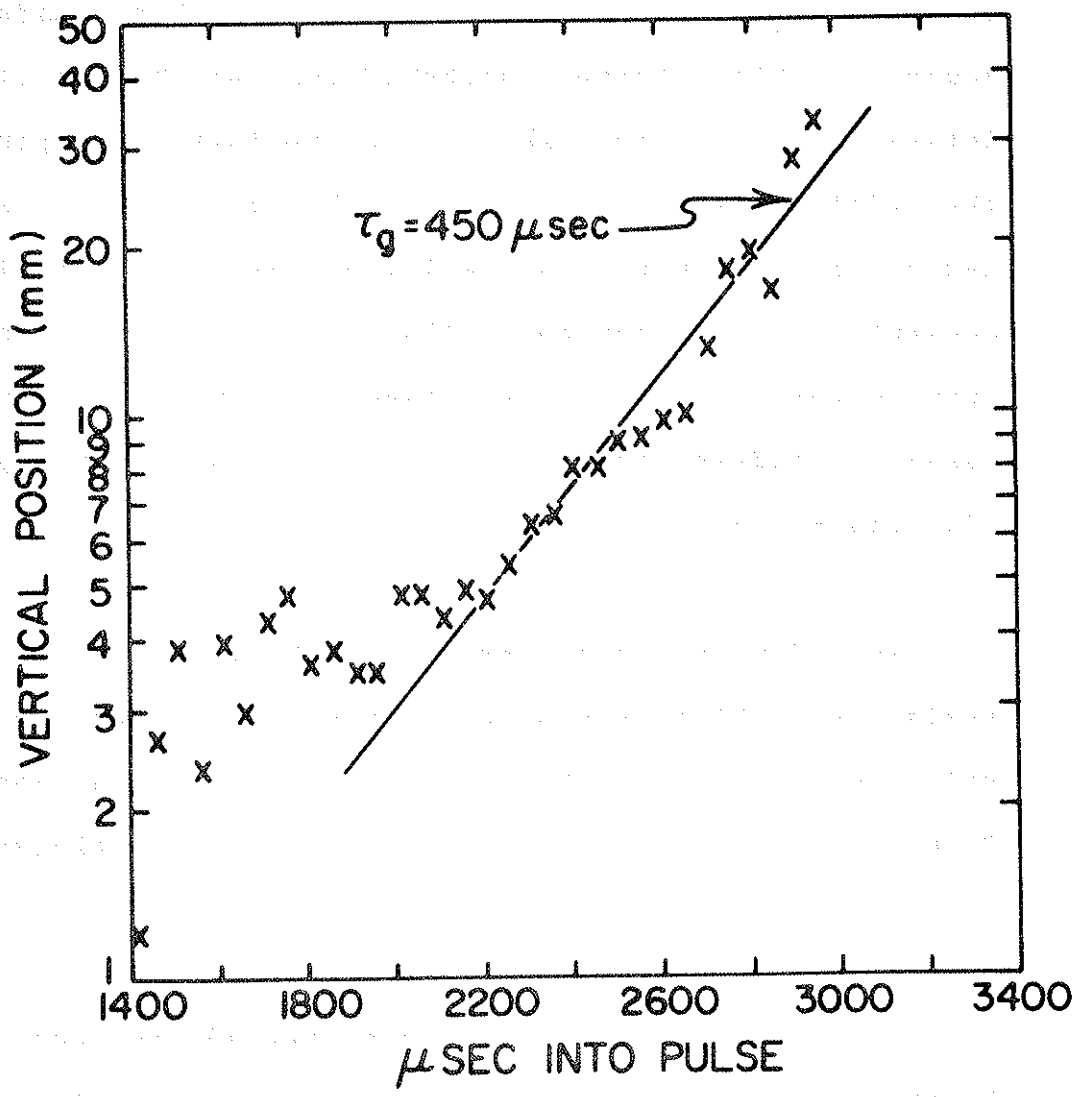

Figure 10: Distance travelled by the magnetic axis as a function of time. Uncertainty in distance travelled is 1-2 mm. 100 μsec= 500 poloidal Alfvén times.

involved. Wooton et. al.[14] found the plasma growth time of an axisymmetric instability in TOSCA to be slowed down by the resistive decay of induced stabilizing currents in the walls and external field shaping coils. The equivalent theoretical prediction has been made[8,13]. However, all these calculations assume an ideal, infinitely conducting plasma. In the Tokapole experiment the finite plasma resistivity (L/R time ~ 1 msec) is the major contributor to the damping of induced stabilizing currents. The rings and walls in this experiment have a much longer resistive decay time (15 msec.) than the plasma. Indeed, instability growth occurs on the plasma L/R time scale.

To address this issue we changed the plasma resistance while keeping the plasma inductance and shape relatively constant. Resistivity profiles are obtained from current and electric field profiles disussed in section III.C.

The resistivity profile was varied in two ways: First, by lowering the toroidal magnetic field which lowers the plasma current. Second, by puffing Ar gas, in addition to the normal H_2, to increase Z_{eff} directly. In either case the electric field profile stayed relatively